

Nonequilibrium thermometry via an ensemble of initially correlated qubits

Enrico Trombetti,¹ Marco Pezzutto,¹ Marco Malitesta,^{1,2} and Stefano Gherardini^{1,3}

¹*Istituto Nazionale di Ottica del Consiglio Nazionale delle Ricerche (CNR-INO), Largo Enrico Fermi 6, I-50125 Firenze, Italy.*

²*Department of Physics and Astronomy, Università di Firenze, Via Sansone 1 I-50019 Sesto Fiorentino, Italy.*

³*European Laboratory for Non-linear Spectroscopy,
Università di Firenze, I-50019 Sesto Fiorentino, Italy.*

(Dated: July 8, 2025)

We investigate a nonequilibrium quantum thermometry protocol in which an ensemble of qubits, acting as temperature probes, is weakly coupled to a macroscopic thermal bath. The temperature of the bath, the parameter of interest, is encoded in the dissipator of a Markovian thermalization process. For some relevant initial states, we observe a peak in the Quantum Fisher Information (QFI) during the transient of the thermalization, indicating enhanced sensitivity in early-time dynamics. This effect becomes more pronounced at higher bath temperatures and is further enhanced when the qubits' initial state has a larger ground-state population. Our analysis shows that both local coherence in the probes' initial state and initial correlations among the probes contribute to the amplification of the peak in the QFI, thus improving the precision of the temperature estimation. The influence of quantum correlations emerges as a central feature of this work. Although the dynamics does not permit superlinear scaling of the QFI with the number of probes, we identify the most effective initial states for designing high-precision quantum sensors within this setting. We also provide concrete guidelines for experimental implementations.

I. INTRODUCTION

Quantum metrology can offer significant advantages over its classical counterpart, enabling better accuracy and precision [1, 2]. This is achievable by using quantum sensors that can be engineered at the atomic scale to allow for the resolution of spatial features with high precision [3]. Quantum sensors can also exploit the fragile yet highly sensitive character of quantum superposition, which makes them particularly effective at detecting weak signals (for instance in gravitational wave detectors [4]). Moreover, even quantum entanglement has been recognized as a resource for enhancing metrological performance when operating in a multi-probe setting, with a possible superlinear scaling of precision with the number of probes [5]. As discussed below, similar advantages can also be obtained in quantum thermometry, which has the goal to estimate with high precision the temperature of a macroscopic thermal bath using quantum systems as thermometers [6, 7].

Among the first models of thermometry in the quantum regime we mention [8, 9] where a qubit is used to probe the temperature of a micromechanical resonator, modelled as a quantum harmonic oscillator. This scenario has been also explored further in the nonlinear optomechanical regime [10]. In this paper, we set our analysis in the context of qubit thermometers [11, 12], which have been experimentally tested in Refs. [13, 14] on a quantum optics platform. Other notable examples include non-destructive thermometry of a Bose-Einstein condensate using impurities as quantum thermometer [15], thermometry of ultracold atoms via nonequilibrium work distributions [16], non-destructive thermometry of cold Fermi gases [17], thermometry of superconducting quantum circuits [18], pairs of trapped ions used as thermometers [19], and even biological ap-

plications of quantum thermometry with cells [20, 21].

The interaction between one or more quantum thermometers and the thermal bath causes the thermometers to thermalize over time. In this setting, the key physical quantity used to quantify the precision for estimating the temperature of the bath at any time t is the Quantum Fisher Information (QFI) built over the thermometers' state. Recent studies [22–24] have highlighted the advantages of measurement strategies performed in nonequilibrium regimes, where the quantum probes are measured before reaching their (local) thermal equilibrium. Measuring before reaching thermal equilibrium offers a twofold advantage: first, it can be faster than the usual equilibrium thermometry, as the measurements of probes are performed before their thermalization has occurred. Secondly, it can allow for significantly more accurate estimates of the bath's temperature.

Further advantages can be given by exploiting quantum resources. For example, in Ref. [24] the authors demonstrated that the presence of quantum coherence in the initial state of a probe can boost the value of the QFI during transient of the thermalization dynamics, thus leading to improved temperature sensitivity at finite times. Moreover, in Ref. [25], a collisional thermometry framework is introduced, where a quantum probe is employed to infer the temperature of a thermal bath. The probe interacts sequentially with a series of N auxiliary systems that correlate over time. The information about the temperature of the bath is extracted from the state of the auxiliary systems whose QFI is shown to scale superlinearly with N . Furthermore, in Ref. [26], fermionic probes strongly coupled to a thermal bath are considered to carry out quantum thermometry. Due to the strong coupling, the probes undergo a non-Markovian dynamics, which proves to be helpful in achieving a higher QFI compared to the one obtained in the Markovian limit of

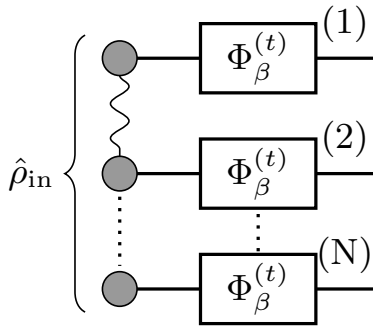


FIG. 1: Quantum-map representation of the system-environment interaction. The system consists of an ensemble of N qubits operating as quantum thermometers. The environment is a thermal bath with unknown inverse temperature β . Each qubit thermometer undergoes thermalization governed by the local map $\Phi_{\beta}^{(t)}$. The ensemble is initially prepared in a quantum-correlated state $\hat{\rho}_{\text{in}}$.

the dynamics. The case of a two-fermion probe is also analyzed, and it is found that, under specific conditions, the QFI can be superadditive due to quantum correlations in the state of the two fermions. Ref. [27] discusses the possibility to carry out quantum thermometry by means of a Lipkin-Meshkov-Glick critical system of up to four particles that is allowed to thermalize. Here, the authors show that, by tuning the anisotropy in the model and the external magnetic field, it is possible to maximize the QFI even up to achieving the ultimate bound to the precision of thermometry. In spite of these efforts, a general understanding of the interplay between multipartite correlations in the initial thermometers' state and performing quantum thermometry in a nonequilibrium regime is still an open research area.

In this paper we aim to understand the conditions under which the precision to get the estimates of temperature is improved using an ensemble of qubits that are quantum-correlated before they interact with the thermal bath; see also Fig. 1. These improvements in precision are to be understood in comparison with that of equilibrium thermometry. In our analysis, we will assume to perform the thermometry during the transient of the qubits' dissipative dynamics due to the weak coupling with the thermal bath. It is worth noting that this is not the usual setting of a quantum metrology experiment where the encoding of the unknown parameter is usually carried out through the unitary evolution of the (closed, quantum) system. Here, within the quantum thermometry context, the information about the temperature of the thermal bath is encoded in the dissipative part of the thermometers' dynamics leading to their thermalization.

By employing multiple thermometers, we investigate how initial quantum correlations among them can enhance the precision of estimating the temperature of the bath during the thermalization dynamics of the thermometers. In the following, we discuss also the role

played on the best achievable precision by the effective local temperature and coherence of thermometers' local states, in relation with the temperature of the thermal bath. To do this, we perform numerical evaluations of the QFI and related quantities using suitably chosen initial states, described in detail in Sec. III. Except for the product state, all the considered initial states are superpositions or mixtures containing the GHZ state [28, 29]. Our numerical results suggest that both local coherences and correlations can improve the performance of nonequilibrium thermometry, as evidenced by an enhancement of the peak in the QFI during the transient dynamics, which surpasses the asymptotic value of the QFI reached once the thermalization is complete. Interestingly, this enhancement is particularly pronounced for high values of the bath temperatures.

Furthermore, although a superlinear asymptotic scaling with the number N of thermometers cannot be achieved by the considered Markovian thermalization map, we study the scaling behavior of the QFI with N . For small values of N , however, initializing the ensemble of thermometers in a quantum correlated state leads to a small deviation of the scaling from the strictly linear one that is achieved in the large- N limit, still provided that the thermometry is performed during the transient of the thermalization dynamics.

II. MODEL

The physical setting considered in this paper is pictorially represented in Fig. 1. The probe system S is composed of N qubits and each of them is a quantum thermometer that is used for estimating the temperature of a thermal bath, i.e., the environment E . The latter is characterized by the inverse temperature $\beta = 1/(k_B T)$, where the Boltzmann constant k_B is fixed to 1 from here on for convenience.

We assume that each qubit interacts weakly with the thermal bath and evolves independently from the others. The dynamics of each qubit thermometer is described by a local Markovian map, as shown in Fig. 1. The coherent dynamics of each qubit thermometer is governed by the following Hamiltonian:

$$\hat{H} = -\frac{\hbar\omega}{2}\hat{\sigma}_z, \quad (1)$$

whose eigenstates are $|0\rangle, |1\rangle$, corresponding to the energies (eigenvalues) $\varepsilon_0 = -\hbar\omega/2$ and $\varepsilon_1 = +\hbar\omega/2$, respectively; from here on, both the reduced Planck constant \hbar and ω are set to 1. We denote the thermal state of a qubit at inverse temperature μ as $\hat{\rho}_{\text{th}}(\mu)$, with $\pi_0(\mu)$ and $\pi_1(\mu)$ representing the corresponding diagonal elements (occupation populations of each energy level):

$$\hat{\rho}_{\text{th}}(\mu) = \begin{pmatrix} \pi_0(\mu) & 0 \\ 0 & \pi_1(\mu) \end{pmatrix}, \quad (2)$$

where $\pi_k(\mu) = e^{-\mu\varepsilon_k}/Z_\mu$ with $k = 0, 1$ and $Z_\mu = e^{-\mu\varepsilon_0} + e^{-\mu\varepsilon_1}$ is the partition function.

The state of each qubit thermometer, subjected to the interaction with the thermal bath with inverse temperature β , tends asymptotically to the thermal state $\hat{\rho}_{\text{th}}(\beta)$, according to the thermalization quantum map $\Phi_\beta^{(t)}$. We assume that the fixed point of the map is the thermal state $\hat{\rho}_{\text{th}}(\beta)$ regardless of the initial state (density operator) $\hat{\rho}(0)$ of each thermometer. As a result, the thermalization of the single thermometer's state is returned by

$$\hat{\rho}_\beta(t) = \Phi_\beta^{(t)}[\hat{\rho}(0)] \text{ such that } \lim_{t \rightarrow +\infty} \Phi_\beta^{(t)}[\hat{\rho}(0)] = \hat{\rho}_{\text{th}}(\beta) \quad (3)$$

for any $\hat{\rho}(0)$. As the dynamical maps act only locally on each qubit thermometer, independently of the others, the evolution of an initial state $\hat{\rho}_{\text{in}}$ for the ensemble of N thermometers is given by the tensor product of N identical maps. This means that, under the assumptions above, every initial state $\hat{\rho}_{\text{in}}$ asymptotically tends to the tensor product of N single-qubit thermal states at the (inverse) temperature of the bath: $\hat{\rho}_{\text{th}}^{\otimes N}(\beta)$. In addition, no correlation can emerge as a consequence of the time evolution. If the quantum map is Markovian, as considered in the following, quantum correlations present in the initial state of the ensemble vanish exponentially over time as an effect of the thermalization dynamics.

A. Generalized amplitude damping map

We consider the thermalization dynamics of an ensemble of N qubit thermometers, each undergoing the interaction with a thermal bath with unknown temperature. We describe this interaction by means of a Generalized Amplitude Damping (GAD) quantum channel in Kraus representation. The Kraus operators defining the channel for the state of the whole ensemble are built through all possible tensor products of the N single-qubit Kraus operators, as detailed below in Sec. II A 1.

The set of Kraus operators describing the time evolution of each qubit thermometer is $\mathcal{K} \equiv \{\hat{K}_1, \hat{K}_2, \hat{K}_3, \hat{K}_4\}$ with

$$\begin{aligned} \hat{K}_1 &= \sqrt{q} \begin{pmatrix} 1 & 0 \\ 0 & \sqrt{1-p} \end{pmatrix}, & \hat{K}_2 &= \sqrt{q} \begin{pmatrix} 0 & \sqrt{p} \\ 0 & 0 \end{pmatrix}, \\ \hat{K}_3 &= \sqrt{1-q} \begin{pmatrix} \sqrt{1-p} & 0 \\ 0 & 1 \end{pmatrix}, & \hat{K}_4 &= \sqrt{1-q} \begin{pmatrix} 0 & 0 \\ \sqrt{p} & 0 \end{pmatrix}, \end{aligned} \quad (4)$$

where p and q are dynamical parameters, function of the inverse temperature β , whose physical meaning will be discussed later. The transformation $\hat{\rho}_0 \mapsto \hat{\rho} = \sum_{i=1}^4 \hat{K}_i \hat{\rho}_0 \hat{K}_i^\dagger$ describes how the initial single-qubit density operator

$$\hat{\rho}_0 = \begin{pmatrix} 1 - \rho_{22} & \rho_{12} \\ \rho_{12}^* & \rho_{22} \end{pmatrix} \quad (5)$$

changes when the GAD channel is applied. This transformation leads to the evolved state

$$\hat{\rho} = \begin{pmatrix} pq + (1-p)(1-\rho_{22}) & \sqrt{1-p}\rho_{12} \\ \sqrt{1-p}\rho_{12}^* & (1-q)p + (1-p)\rho_{22} \end{pmatrix}. \quad (6)$$

This dynamics can be generated equivalently also by the Gorini-Kossakowski-Lindblad-Sudarshan quantum master equation

$$\frac{\partial \hat{\rho}}{\partial t} = -\frac{i}{\hbar} [\hat{H}, \hat{\rho}] + \sum_{j \neq k} \left(\hat{\mathcal{L}}_{jk} \hat{\rho} \hat{\mathcal{L}}_{jk}^\dagger - \frac{1}{2} \{ \hat{\mathcal{L}}_{jk}^\dagger \hat{\mathcal{L}}_{jk}, \hat{\rho} \} \right), \quad (7)$$

where \hat{H} is the qubit Hamiltonian (1) and $\hat{\mathcal{L}}_{ij}$ are the jump operators responsible for the Markovian thermalization dynamics, which read as

$$\hat{\mathcal{L}}_{jk} = \sqrt{\Gamma_{jk}} |j\rangle\langle k|, \quad j, k \in \{0, 1\}. \quad (8)$$

In (8),

$$\Gamma_{jk} = \begin{cases} \gamma(n_{jk} + 1) & j < k \\ 0 & j = k \\ \gamma n_{jk} & j > k. \end{cases} \quad (9)$$

are the transition rates from state k to state j , with $\gamma > 0$ denoting the evolution rate of the single thermometer, while n_{jk} are the thermal ratios $n_{jk} = 1/(e^{\beta(\varepsilon_k - \varepsilon_j)} - 1)$.

The solution of the quantum master equation (7) evolves the single-qubit density operator $\hat{\rho}_0$ of Eq. (5) into the time-dependent state $\hat{\rho}_\beta(t)$ equal to

$$\begin{pmatrix} (1 - e^{\lambda t})\pi_0 + e^{\lambda t}(1 - \rho_{22}) & e^{-it + \frac{\lambda t}{2}} \rho_{12} \\ e^{it + \frac{\lambda t}{2}} \rho_{12}^* & (1 - e^{\lambda t})\pi_1 + e^{\lambda t} \rho_{22} \end{pmatrix} \quad (10)$$

with $\pi_1 = 1 - \pi_0$. Eqs. (6) and (10) provide the same quantum state apart from the off-diagonal phase e^{-it} stemming from the coherent dynamics $i[\hat{H}, \hat{\rho}]/\hbar$ in (7). This similarity allows us to determine the physical meaning of the parameters p, q . In Eq. (10), $\pi_0 = \pi_0(\beta)$ (resp. $\pi_1 = \pi_1(\beta)$) is the thermal population at the temperature of the bath associated to the ground state (resp. excited state) of the thermometer, while λ is the coefficient that defines the thermalization rate of the dynamics. The latter is given by

$$\lambda = \frac{\gamma}{\pi_1(\beta) - \pi_0(\beta)} = -\gamma \coth\left(\frac{\beta \hbar \omega}{2}\right) \quad (11)$$

and it is always negative when a well-defined positive bath temperature is considered. Hence, if we neglect the oscillations in the off-diagonal terms in Eq. (10), the thermalization process can be described by the GAD channel of Eq. (6) by setting $q = \pi_0(\beta)$ and $p = 1 - e^{\lambda t}$. The resulting fixed point of the channel, obtained in the limit of $t \rightarrow +\infty$, is $\text{diag}[q, 1 - q]$ that correctly corresponds to the thermal state $\text{diag}[\pi_0(\beta), \pi_1(\beta)]$. Before proceeding, it is worth noting that to each thermometer, being a

qubit, we can associate at any time t a local temperature T_q that concerns the population terms of its state. In the following, we will explicitly consider only the local temperature associated to the initial state of the thermometers, defined by

$$T_q = \frac{\varepsilon_1 - \varepsilon_0}{\ln\left(\frac{1 - \rho_{22}}{\rho_{22}}\right)}. \quad (12)$$

From both Eqs. (6) and (10) it is evident that the considered thermalization channel evolves the diagonal and off-diagonal terms of the single-qubit density operator independently. Therefore, the population and coherence components of each qubit thermometer undergo independent thermalization dynamics characterized by distinct dissipation rates. The exponential factors governing the thermalization of the diagonal and off-diagonal elements of each thermometer's state differ by a factor $1/2$.

It is worth noting that the ensemble of thermometers acquires information about the temperature β of the thermal bath through its dynamical interaction with the environment. In fact, the Lindblad formalism clearly shows that this information is carried exclusively by the dissipative component of the dynamics. We would like to stress that this is not the typical setting in quantum metrology, where the parameter to be estimated is usually encoded through a unitary evolution of the system, and open-system effects are introduced merely as perturbations or disturbances to the encoding unitary dynamics.

1. Time-evolution of a multi-qubit state

The nonequilibrium thermometry setting, which we are referring to, considers a model where the interaction between each qubit thermometer and the thermal bath is local and independent. Consequently, the evolution map of an ensemble of these thermometers is obtained by applying N independent quantum channels $\Phi_\beta^{(t)}$:

$$\hat{\rho}_{\text{out}}(t, \beta) = \left(\Phi_\beta^{(t)}\right)^{\otimes N} [\hat{\rho}_{\text{in}}], \quad (13)$$

where $\hat{\rho}_{\text{in}}$ and $\hat{\rho}_{\text{out}}(t, \beta)$ are the initial and evolved (at time t) states of the ensemble, respectively. Hence, given the Kraus representation of the single-qubit channel in terms of the set of operators \mathcal{K} , the time-evolution of the ensemble of N qubit thermometers is described by the set

$$\mathcal{K}_N \equiv \left\{ \hat{K}_a(N) = \bigotimes_{i=1}^N \hat{K}_j^{(i)}, j = 1, 2, 3, 4 \right\}_{a=1}^{4^N} \quad (14)$$

that contains 4^N Kraus operators overall. The corresponding asymptotic N -qubit state is a separable state,

whose reduced states associated to each qubit thermometer are all equal to the thermal state at the inverse temperature β of the bath:

$$\lim_{t \rightarrow +\infty} \left(\Phi_\beta^{(t)}\right)^{\otimes N} [\hat{\rho}_{\text{in}}] = \hat{\rho}_{\text{th}}^{\otimes N}(\beta) \quad \forall \hat{\rho}_{\text{in}}. \quad (15)$$

III. INPUT STATES

In our analysis we consider a class of relevant input states $\hat{\rho}_{\text{in}}$, all defined over N qubits and possibly including quantum correlations among the qubits. Each state is characterized by distinct parameters and exhibits specific features, whose differences will be discussed below. In the numerical evaluations we are going to show, the number N of qubits in the ensemble of thermometers ranges up to six.

a. Product states. A generic parametrization for the density operator of the single qubit thermometer is

$$\hat{\rho}_1(a, r, \phi) = \begin{pmatrix} 1-a & \sqrt{a(1-a)}re^{i\phi} \\ \sqrt{a(1-a)}re^{-i\phi} & a \end{pmatrix}, \quad (16)$$

where $a \in [0, 1]$, $r \in [0, 1]$ and $\phi \in [0, 2\pi[$. When $r = 0$, no quantum coherence is present in the state and, consequently, $\hat{\rho}_1$ can be described by a thermal state with an effective inverse temperature specified by the free parameter a . On the other hand, when $r = 1$ the state $\hat{\rho}_1(a, r, \phi)$ is pure and contains the maximum amount of quantum coherence compatible with the choice of a . Thus, we take into account the tensor product of N density operators as given by Eq. (16) to generate the separable state of N qubits

$$\hat{\rho}_{\text{ps}}(a, r, \phi) = \hat{\rho}_1(a, r, \phi)^{\otimes N}. \quad (17)$$

For $a = 0$, Eq. (17) simplifies to the state $|0\rangle\langle 0|^{\otimes N}$ that is the ground state of the ensemble of thermometers.

From the analytical expression of the QFI for the generic state (16) discussed in [24], one can observe that the phase ϕ does not affect the value of the QFI, as the off-diagonal elements of the density operator appear in the QFI only through their modulus. Therefore, without loss of generality, we set ϕ to zero.

b. Identity-mixed GHZ states ($\mathbb{1}$ -m). We focus also on the mixture between the density matrix corresponding to the GHZ state

$$|\text{GHZ}_N\rangle = \frac{|0\rangle^{\otimes N} + |1\rangle^{\otimes N}}{\sqrt{2}} \quad (18)$$

and the identity $\mathbb{1}_{2^N}/2^N$ (including the normalization factor $1/2^N$), using weights η and $1 - \eta$, with η being a real number between 0 and 1. Formally, we get:

$$\hat{\rho}_{\mathbb{1}\text{-m}}(\eta) = \eta |\text{GHZ}_N\rangle\langle \text{GHZ}_N| + (1 - \eta) \frac{\mathbb{1}_{2^N}}{2^N}, \quad (19)$$

where the parameter η tunes the amount of correlations between qubits, which grows as η increases. Interestingly, when $N = 2$, these states correspond to isotropic states (see Ref. [30]), which in turn are related to Werner states [31] since applying the partial transposition operation to one of the two subsystems transforms one type of quantum state into the other [32].

An important property of the Identity-mixed states of Eq. (19) is that, regardless of the value of η , the reduced density operator for each qubit is equal to the (normalized) identity operator, which corresponds to a thermal state at infinite temperature:

$$\text{Tr}_{S_{\setminus i}} [\hat{\rho}_{1-m}(\eta)] = \frac{\mathbb{1}_2}{2} \quad \forall i \in \{1, \dots, N\}. \quad (20)$$

In Eq. (20), $S_{\setminus i} \equiv S_1 + S_2 + \dots + S_{i-1} + S_{i+1} + \dots + S_N$, where S_j refers to the subsystem consisting in the j -th qubit.

c. Thermal-mixed GHZ states modified by thermal weights (t-m). These states are similar to the previous ones, but with the addition that we introduce a tunable local temperature of the individual qubits. First of all, to do this, we define the states

$$|\psi_N(\mu)\rangle \equiv \sqrt{\pi_0(\mu)} |0\rangle^{\otimes N} + \sqrt{\pi_1(\mu)} |1\rangle^{\otimes N}, \quad (21)$$

which are superpositions of $|0\rangle^{\otimes N}$ and $|1\rangle^{\otimes N}$ states with respective probabilities given by the thermal populations $\pi_0(\mu)$ and $\pi_1(\mu)$ at inverse temperature μ . Then, we construct the target density operator as a mixture of the density operator associated with $|\psi_N(\mu)\rangle$ and the tensor product of N thermal states at inverse temperature μ :

$$\hat{\rho}_{t-m}(\eta, \mu) = \eta |\psi_N(\mu)\rangle \langle \psi_N(\mu)| + (1 - \eta) \hat{\rho}_{th}^{\otimes N}(\mu), \quad (22)$$

where η tunes the amount of correlations between qubits as in the identity-mixed GHZ states.

Here, the parameter μ corresponds to the local inverse temperature $1/T_q$ of the qubits, whose local states remain again unaffected by the value of η :

$$\text{Tr}_{S_{\setminus i}} [\hat{\rho}_{t-m}(\eta, \mu)] = \hat{\rho}_{th}(\mu) \quad \forall i \in \{1, \dots, N\}. \quad (23)$$

We can observe that when $\mu \rightarrow +\infty$ the ground state $\hat{\rho}_{gs}$ is recovered, while when $\mu \rightarrow 0^+$ we obtain the identity-mixed GHZ state (19).

d. k-GHZ superposition states (k-s). These states are constructed as a superposition of the $|\text{GHZ}_N\rangle$ state and the product state $|k\rangle^{\otimes N}$, where $|k\rangle$ is a generic pure state. The weights of the superposition are given by $\sin \alpha$ and $\cos \alpha$, respectively, divided by the appropriate normalization constant $C(\alpha, k)$ which depends on both α and k . Hence

$$|\psi_{k-s}(\alpha, k)\rangle = \frac{1}{C(\alpha, k)} (\sin(\alpha) |\text{GHZ}_N\rangle + \cos(\alpha) |k\rangle^{\otimes N}) \quad (24)$$

and the density operator associated to this pure state is simply

$$\hat{\rho}_{k-s}(\alpha, k) = |\psi_{k-s}(\alpha, k)\rangle \langle \psi_{k-s}(\alpha, k)|. \quad (25)$$

The parameter α determines the correlations among the qubits—being maximal for the GHZ state and vanishing when the state is fully separable—but it also affects other properties. Specifically, in the following we choose $|k\rangle$ to be one of the eigenstates of the Pauli matrices. When $|k\rangle = |0\rangle, |1\rangle$, the parameter α modifies the local populations, while the local quantum coherence terms are constantly zero. For $|k\rangle$ set as $|\pm\rangle \equiv (|0\rangle \pm |1\rangle)/\sqrt{2}$, α controls the local coherences, while the populations are constant and equal to $1/2$. Finally, for $|k\rangle = |r\rangle \equiv (|0\rangle + i|1\rangle)/\sqrt{2}$ or $|\ell\rangle \equiv (|0\rangle - i|1\rangle)/\sqrt{2}$, both local populations and quantum coherences are affected by α .

e. Squeezed states. Squeezed states are ubiquitous in quantum metrology [33, 34]. They have been realized on a variety of platforms [35] and have enabled improved metrological performance in different technological applications. In the following, we consider the squeezed states generated by the one-axis twisting dynamics [36]. Let us take the N qubit thermometers to be initially in the product state $|+\rangle^{\otimes N}$, and introduce the angular-momentum operators \hat{J}_x, \hat{J}_y , and \hat{J}_z with $\hat{J}_\alpha \equiv \sum_{i=1}^N \sigma_\alpha^{(i)}/2$ for $\alpha = x, y, z$. The one-axis twisting corresponds to the unitary evolution

$$|\psi_{sq}(\chi)\rangle = e^{-i\chi \hat{J}_z^2} |+\rangle^{\otimes N}, \quad (26)$$

where χ can be seen as a parameter that controls the strength of the squeezing process. The associated density operator is

$$\hat{\rho}_{sq}(\chi) = |\psi_{sq}(\chi)\rangle \langle \psi_{sq}(\chi)|. \quad (27)$$

The state $|\psi_{sq}(\chi)\rangle$ is entangled [37] except for the values $\chi = k\pi$ ($k \in \mathbb{N}$) of the squeezing parameter, whereby a product state is obtained. Indeed, the squeezed state—up to a phase factor—is periodic in χ so that we have a complete revival of the initial state for $\chi = \pi$ if N is odd, and for $\chi = 2\pi$ if N is even. We also notice that, for $\chi = \pi/2$, $|\psi_{sq}(\chi)\rangle$ is a rotated- $|\text{GHZ}_N\rangle$ state, which is maximally entangled. A rotated- $|\text{GHZ}_N\rangle$ state is defined as a $|\text{GHZ}_N\rangle$ state that is rotated through an angle $\pi/2$ around the y -axis. In general, as the parameter χ approaches $\pi/2$, the correlations among the qubits that compose the state are enhanced.

In order to introduce a further degree of freedom, we can perform an additional rotation of the state of Eq. (26). We thus define $\hat{\rho}_{sqr}(\chi, \theta) = e^{-i\theta \hat{J}_y} |\psi_{sq}(\chi)\rangle$, where the rotation of $|\psi_{sq}(\chi)\rangle$ is of the angle θ around the y direction. Although $e^{-i\theta \hat{J}_y}$ cannot change the entanglement properties of our system being a local operation, it may still affect the QFI and thus the amount of retrievable information on β . Hence, the initial state of the thermometers' ensemble in this case is $\hat{\rho}_{sqr}(\chi, \theta) = |\psi_{sqr}(\chi, \theta)\rangle \langle \psi_{sqr}(\chi, \theta)|$, which is always pure by construction. The corresponding reduced density operator for

each qubit $i \in \{1, \dots, N\}$ is

$$\begin{aligned} \text{Tr}_{S_{\setminus i}} [\hat{\rho}_{\text{sqr}}(\chi, \theta)] &= \\ &= \frac{1}{2} \begin{pmatrix} 1 - \cos^{N-1}(\chi) \sin(\theta) & \cos^{N-1}(\chi) \cos(\theta) \\ \cos^{N-1}(\chi) \cos(\theta) & 1 + \cos^{N-1}(\chi) \sin(\theta) \end{pmatrix} \end{aligned} \quad (28)$$

as shown in Appendix A.

Eq. (28) highlights the role of the squeezing parameter in determining both the local populations and quantum coherence of the individual subsystems. Notably, when the rotation angle θ around the y-axis is zero, the single-qubit populations are fixed at $1/2$, independently of the value of χ .

IV. QUANTUM FISHER INFORMATION

The Quantum Fisher Information (QFI) is a central tool to assess the maximum achievable precision in the estimation of a parameter—the inverse temperature of the bath β in our case—whose unknown value is encoded into the state of a quantum system [38, 39]. Specifically, the QFI sets a fundamental lower bound on the variance of any unbiased estimator $\tilde{\beta}$ of the parameter β , via the quantum Cramér-Rao bound [38]:

$$\Delta \tilde{\beta} \geq \frac{1}{\sqrt{\nu \mathcal{F}_Q(\hat{\rho}_{\text{out}}(t, \beta))}} \quad (29)$$

where $\Delta \tilde{\beta}$ denotes the standard deviation of $\tilde{\beta}$, ν is the number of independent measurements and $\mathcal{F}_Q(\hat{\rho}_{\text{out}}(t, \beta))$ is the QFI of the evolved state in Eq. (13). The QFI is defined through the Symmetric Logarithmic Derivative (SLD), denoted by \hat{L}_β , which is in turn implicitly defined by the Lyapunov equation

$$\frac{\partial \hat{\rho}_{\text{out}}(t, \beta)}{\partial \beta} = \frac{1}{2} \{ \hat{\rho}_{\text{out}}(t, \beta), \hat{L}_\beta(t) \}. \quad (30)$$

In terms of the SLD, the QFI can be expressed as:

$$\mathcal{F}_Q(\hat{\rho}_{\text{out}}(t, \beta)) = \text{Tr} \left[\frac{\partial \hat{\rho}_{\text{out}}(t, \beta)}{\partial \beta} \hat{L}_\beta(t) \right] \quad (31)$$

Maximizing this quantity is a prerequisite for optimal performance in quantum metrology. In our case, writing

$$\mathcal{F}_Q(\hat{\rho}_{\text{out}}(t, \beta)) = \mathcal{F}_Q \left(\left(\Phi_\beta^{(t)} \right)^{\otimes N} [\hat{\rho}_{\text{in}}] \right) \quad (32)$$

highlights the two relevant quantities to be addressed in the optimization. One is the input state $\hat{\rho}_{\text{in}}$: different $\hat{\rho}_{\text{in}}$ have been considered in Sec. III. The second is the map $\Phi_\beta^{(t)}$ which, depending on the time $t \geq 0$, produces a different encoding of the parameter β on $\hat{\rho}_{\text{in}}$. For $t = 0$, the map $\Phi_\beta^{(t=0)} = \mathbb{1}$ provides no information about β and, indeed, we have $\mathcal{F}_Q(\hat{\rho}_{\text{out}}(t = 0, \beta)) = 0$. For $t \rightarrow +\infty$, the map $\Phi_\beta^{(t \rightarrow +\infty)}$ converts any input states to a thermal

state at bath temperature: $\hat{\rho}_{\text{th}}(\beta)$. Using Eq. (15), the relation $\mathcal{F}_Q(\hat{\rho}_{\text{th}}(\beta)) = \Delta^2 \hat{H}$ valid for thermal states [23, 24, 40], and the additivity of the QFI on separable states, we find

$$\mathcal{F}_Q(\hat{\rho}_{\text{out}}(t \rightarrow +\infty, \beta)) = N \Delta^2 \hat{H}. \quad (33)$$

For the Hamiltonian in Eq. (1), the thermal variance is found to be $\Delta^2 \hat{H} = (\varepsilon_1 - \varepsilon_0)^2 \pi_0(\beta) (1 - \pi_0(\beta))$ (see Appendix B for details). Therefore, at thermal equilibrium, the ultimate achievable precision is fundamentally limited by the bath temperature through the thermal population $\pi_0(\beta)$. Even initial quantum correlations between qubits are of no advantage in this regime, as they are completely washed out by the thermalization process according to Eq. (15). This motivates our investigation of the non-equilibrium transient regime, where larger QFI than Eq. (33) can in fact be attained.

A. Upper bound and scaling with qubit number

The role of $\Phi_\beta^{(t)}$ is further clarified by introducing the *channel QFI*, defined as [41]:

$$\mathcal{F}_Q \left(\Phi_\beta^{(t)} \right) = \max_{\hat{\rho}_{\text{in}}} \mathcal{F}_Q \left(\left(\Phi_\beta^{(t)} \right)^{\otimes N} [\hat{\rho}_{\text{in}}] \right). \quad (34)$$

This describes a limit on precision that comes solely from the parameter-encoding map $\Phi_\beta^{(t)}$. It can be interpreted as quantifying how effective the temperature encoding realized by the selected channel is at different times during thermalization. For a unitary encoding channel: $\hat{U}_\beta = e^{-i\beta \hat{H}}$, the optimization in Eq. (34) is easily performed, yielding the quadratic scaling with qubit number N popularly known as *Heisenberg scaling* [42]. Optimal states $\hat{\rho}_{\text{in}}$ for unitary channels are typically highly-entangled pure states such as the GHZ state in Eq. (18). Unfortunately, in the presence of decoherence, an equally nice and simple solution is generally not available. Maximizing the QFI becomes a much more challenging task, and achieving quadratic scaling with N may not always be possible. However, it is possible to approximate the channel QFI using a more computationally accessible upper bound, which is saturable only for specific maps and under special conditions [42, 43]:

$$\mathcal{F}_Q \left(\Phi_\beta^{(t)} \right) \leq 4 \min_{\mathcal{K}'} \left[N \left\| \hat{M}_1(\mathcal{K}') \right\| + N(N-1) \left\| \hat{M}_2(\mathcal{K}') \right\|^2 \right]. \quad (35)$$

In the above equation, the minimization is performed over all equivalent Kraus representations $\mathcal{K}' \equiv \{\hat{K}'_a\}_{a=1, \dots, l}$ of the map $\Phi_\beta^{(t)}$: recall that two representations $\mathcal{K} \equiv \{\hat{K}_a\}_{a=1, \dots, l}$ and $\mathcal{K}' \equiv \{\hat{K}'_a\}_{a=1, \dots, l}$ are equivalent if it exists a unitary matrix U_{ab} (which may depend on β) such that $\hat{K}'_a = \sum_b U_{ab} \hat{K}_b$ for $a, b = 1, \dots, l$. The symbol $\|\cdot\|$ represents the operator norm, and \hat{M}_1 and \hat{M}_2

are defined in terms of the generic Kraus representation \mathcal{K}' as:

$$\hat{M}_1(\mathcal{K}') = \sum_a \frac{\partial \hat{K}'_a{}^\dagger}{\partial \beta} \frac{\partial \hat{K}'_a}{\partial \beta}, \quad \hat{M}_2(\mathcal{K}') = i \sum_a \frac{\partial \hat{K}'_a{}^\dagger}{\partial \beta} \hat{K}'_a. \quad (36)$$

We remark that the upper bound in Eq. (35) assumes initial states $\hat{\rho}_{\text{in}}$ that are independent of the parameter to be estimated. Later in this work, we will further analyze this bound and characterize the ultimate scaling of precision achievable within our scheme.

V. RESULTS

We now present the results of our analysis, focusing on how specific features of the initial state influence the QFI. In particular, we describe the effects of the bath temperature, the local temperature [refer to Eq. (12)], the coherence of the reduced states of the thermometers, and the correlations among them. In the following, the state correlation of two-qubit bipartite systems is quantified by means of the *negativity of entanglement* [44], which we compute as

$$\mathcal{N} \equiv \left| \sum_{\lambda_i < 0} \lambda_i \right|, \quad (37)$$

where λ_i are the eigenvalues of the partially transposed density operator of the whole thermometers' state with respect to one of the two qubits composing it. Then we examine how the QFI scales with the number of thermometers N by analyzing the behavior of its maximum value. We recall that the asymptotic value of the QFI depends only on the bath temperature, therefore any differences in the values of the QFI due to the features of the initial state $\hat{\rho}_{\text{in}}$ can be appreciated only during the transient of the dynamic for fixed β and N .

These evaluations are primarily carried out using the Wolfram Mathematica software [45]. The state evolution is implemented analytically, explicitly retaining the dependence of the states on time and on the inverse temperature of the bath. This approach allows for the analytical computation of the derivative of the state with respect to the parameter to be estimated (the inverse temperature β). This derivative is required to solve the Lyapunov equation (30) and determine the Symmetric Logarithmic Derivative (SLD). This step, as well as the final numerical evaluation of the QFI, is performed numerically. The plots presented in the following are also generated using the same software.

For the following discussion, it is useful to introduce the quantities

$$v_\varphi^{(\max)}(\Phi_\beta^{\otimes N}, \hat{\rho}_{\text{in}}) = \max_t \mathcal{F}_Q \left(\Phi_\beta^{\otimes N} [\hat{\rho}_{\text{in}}(\varphi_{\max})] \right) \quad (38)$$

$$v_\varphi^{(\min)}(\Phi_\beta^{\otimes N}, \hat{\rho}_{\text{in}}) = \max_t \mathcal{F}_Q \left(\Phi_\beta^{\otimes N} [\hat{\rho}_{\text{in}}(\varphi_{\min})] \right) \quad (39)$$

where $\varphi \in [\varphi_{\min}, \varphi_{\max}]$ is a variable of interest in $\hat{\rho}_{\text{in}}$. Eqs. (38)-(39) correspond to the maximum of the QFI (in time) for the maximum and the minimum of the variable φ , respectively; the values of all the other variables in $\hat{\rho}_{\text{in}}$ are considered fixed. Thus, one can define the ratio

$$v_\varphi(\Phi_\beta^{\otimes N}, \hat{\rho}_{\text{in}}) \equiv \frac{v_\varphi^{(\max)} - v_\varphi^{(\min)}}{v_\varphi^{(\max)}}, \quad (40)$$

which is the relative change in the maximum value of the QFI, evaluated at the endpoints of the range of the variable φ .

A. The role of bath and thermometers' temperatures

We begin by analyzing how the QFI depends on the temperature of the bath, using states defined on two qubits. As shown in Fig. 2, the QFI exhibits an earlier and more marked peak during the transient when the bath temperature is higher. This behavior indicates enhanced sensitivity of the qubit thermometers when probing a hot bath compared to a cold one. Regardless of the thermometers' local temperature, the enhancement of the maximum value taken by the QFI (when it is greater than the corresponding asymptotic value) scales superlinearly with the temperature T of the bath. Moreover, the time needed by the QFI for converging to the asymptotic value decreases as the bath temperature increases. This result is consistent with our predictions, since the thermalization is governed by the exponential of $\lambda t = -|\lambda|t$. The magnitude of λ increases for smaller values of β [cfr. Eq. (11)], which leads to faster relaxation of each thermometer to the thermal equilibrium.

We now analyze the role of the local temperature of the thermometers on the behavior of the QFI. At first, we consider a thermal initial state defined on a single qubit, parametrized as in (16) with $r = 0$, while its temperature (encoded by the parameter a) varies. For a more detailed discussion, we refer to Ref. [24] where this analysis has been already conducted. When a increases from 0 to $1/2$, corresponding to an increase of the thermometers' temperature from 0 to $+\infty$, the maximum value of the QFI decreases. Specifically, at low temperatures, a pronounced peak in the QFI emerges during the transient. This peak becomes less prominent and eventually disappears as a increases. For values of a between $1/2$ and 1, associated with population inversion and negative temperatures of the thermometers, a local maximum in the QFI is again observed in the transient regime. However, this peak is smaller in absolute value compared to the low positive temperature case, and is followed by a drop in the QFI before the latter monotonically approaches its asymptotic thermal value.

We now extend our analysis about the influence of the local qubit temperature to the case of multiple thermometers. We find that, also in this case, a reduction

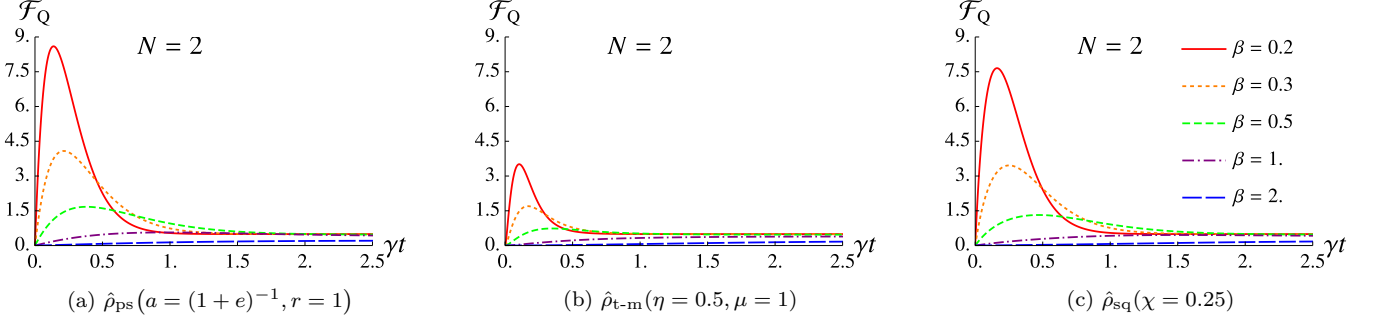


FIG. 2: QFI of the evolved state of an ensemble of 2 qubits initialized in different states. Different colors correspond to different bath temperatures. The initial states employed in panels (a) and (b) share the same local temperatures; those in panels (b) and (c) exhibit the same negativity of entanglement; and the initial states employed for panels (a) and (c) are both pure. All the plots display comparable behavior depending on the bath's inverse temperature.

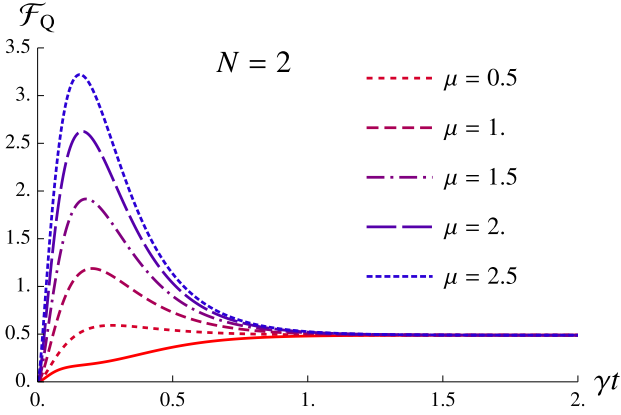


FIG. 3: QFI of the evolved thermometers' ensemble state, initialized in the thermal-mixed GHZ state modified by thermal weights $\hat{\rho}_{t-m}$ (22). Different colors correspond to different values of the local thermometers' inverse temperature μ . The inverse temperature of the bath is $\beta = 0.3$ and the correlation parameter is $\eta = 0.2$.

in the local temperature of each thermometer's reduced state has a positive impact on the QFI. To verify this effect, let us consider the identity-mixed GHZ states modified by thermal weights (t-m) $\hat{\rho}_{t-m}$ (refer to paragraph c. of Sec. III). The corresponding results for fixed values of η and bath inverse temperature β are shown in Fig. 3. From the figure, indeed, we can observe that for fixed $\beta = 0.5$ the QFI increases monotonically as μ increases, where μ corresponds to the local inverse temperature of the single thermometer.

Another insightful perspective is provided by Fig. 4, which shows the difference between the maximum value of the QFI and its asymptotic value as a function of the inverse temperature of the two qubits. In this case, we set $\eta = 0$ in order to eliminate the contribution of correlations to the QFI, effectively working with a tensor product of two thermal state with inverse temperature μ

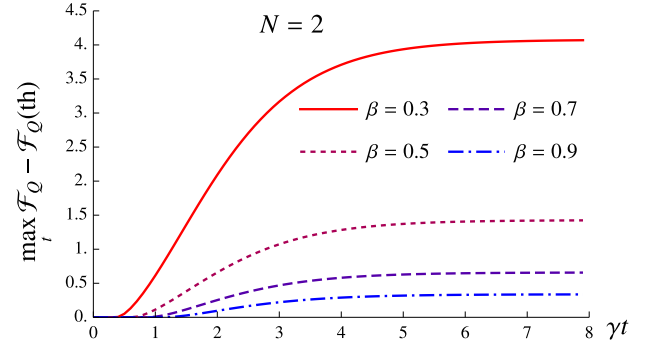


FIG. 4: $\max_t \{ \mathcal{F}_Q(\Phi_\beta^{(t)}[\hat{\rho}_{t-m}(\eta=0, \mu)]) \} - \mathcal{F}_Q(\hat{\rho}_{th}(\beta))$ as a function of the local inverse temperature μ of the qubits. By choosing $\eta = 0$ the thermometers' state is initialized in a product of single-qubit thermal states. Different colors correspond to different inverse bath temperatures β .

(the role of correlations is discussed in Sec. V C). One can observe that, under the conditions of Fig. 4, the maximum value of the QFI coincides with its asymptotic value until the local temperature of the qubits reaches a critical point, beyond which a transient peak emerges. The discrepancy between the maximum and the asymptotic values of the QFI increases monotonically with β , reaching its largest value as the initial state approaches the ground state at zero temperature, for large values of μ .

Finally, we employ the quantifier $v_\mu(\Phi_\beta^{\otimes 2}, \hat{\rho}_{t-m})$ as defined in Eq. (40) to evaluate the relative gain in the QFI induced by the parameter μ , as a function of the bath inverse temperature β , for different values of the correlation parameter η . Specifically, μ ranges from zero, corresponding to the ground state, to $+\infty$, where the state approaches the $\hat{\rho}_{1-m}(\eta)$ state (19). As shown in Fig. 5, v_μ increases with β as long as the $\hat{\rho}_{1-m}(\eta)$ state exhibits, during the transient, a peak in the QFI that exceeds its asymptotic value. On the other hand, in the

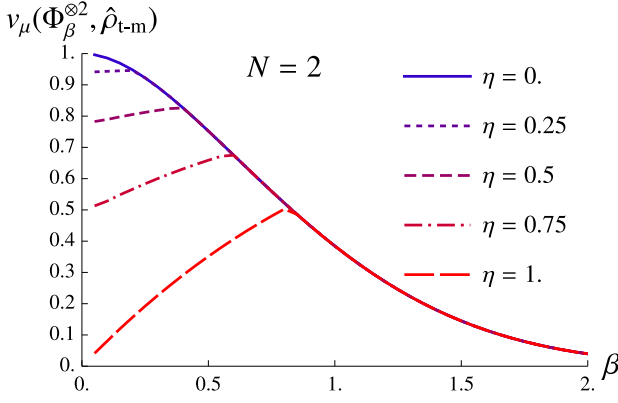


FIG. 5: Relative enhancement $v_\mu(\Phi_\beta^{\otimes 2}, \hat{\rho}_{t-m})$ (40) of QFI w.r.t. the local thermometers' inverse temperature μ , as a function of the inverse bath temperature β . Initial state: thermal-mixed GHZ state modified by thermal weights (22). Different colors correspond to different values of the correlation parameter $\eta \in [0, 1]$.

regime where the QFI of the $\hat{\rho}_{1-m}(\eta)$ reaches its maximum value at thermalization, the function v_μ begins to decrease, independently from the value of η (as the latter does not affect the asymptotic value of the QFI).

B. The role of quantum coherence

Let us investigate how the local coherences of the individual thermometer of the ensemble affect the QFI. The product state $\hat{\rho}_1(a, r, \phi)$ of Eq. (16) is used as the initial state for this analysis, where the parameter r tunes the local coherences. Notice that, for simplicity, the analysis is carried out using the single-qubit product state since the results for N qubits can be obtained by rescaling the values of the single-qubit QFI by a factor N , due to the additivity property of the QFI for separable states.

As discussed in Ref. [24], once fixed the value of a (apart from $a = 0$ and $a = 1$), having r larger than zero linearly enhances the quantum coherence and leads to a higher value of the QFI in the transient. This is true for all possible values of the bath temperature. Because of the adopted parametrization, this improvement is differently pronounced depending on the value of a : for $a = 0$ there is no improvement; instead, the improvement is the greatest for $a = 1/2$, for which, when $r = 1$, the amount of quantum coherence is maximized.

In Fig. 6, we quantify the impact that the coherence has on the maximum value of the QFI depending on the value of the bath temperature. To do this, we use the quantity $v_r(\Phi_\beta, \hat{\rho}_{in})$ defined in Eq. (40) with $\hat{\rho}_{in} = \hat{\rho}_{ps}$. Notably, this quantity is independent of N for any initial separable state, and thus even for the initial product state we are considering. As shown in Fig. 6, the enhancement of the QFI due to local coherence is more significant at higher bath temperatures (small β), while

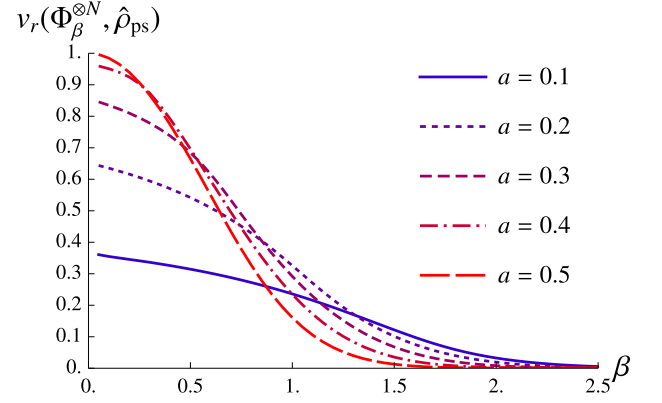


FIG. 6: Relative enhancement $v_r(\Phi_\beta, \hat{\rho}_{ps})$ (40) of QFI w.r.t. the thermometer coherence parameter r (16), as a function of the inverse bath temperature β . This quantity does not depend on the number N of thermometers. Different colors correspond to different values of the initial population parameter $a \in [0, 1/2]$.

it becomes negligible as the temperature decreases. It is also interesting to observe that the relative improvement due to r , quantified by v_r , is more pronounced when a is closer to (but still less than) $1/2$. This improvement is apparent for a narrower range of β values as a increases, entailing that v_r decreases monotonically with β more rapidly for larger values of a .

C. The role of quantum correlations

We now analyze the effect due to initial correlations among the probes on the QFI during the transient of the dynamics, which represents the main novel contribution of this work.

We begin by considering the $\hat{\rho}_{1-m}$ state (19) of 2 qubits as the initial state of the thermometers' ensemble. The QFI of the evolved state is shown in Fig. 7 for various values of the parameter η , which controls the presence of correlation. It is evident that the QFI increases with η before the thermometers reach the thermal equilibrium. For sufficiently large values of the parameter, a peak in the QFI emerges during the thermalization transient, thus surpassing the asymptotic value reached in the long-time regime. This peak becomes more pronounced as the correlations grow, reaching its maximum for $\eta = 1$, for which the initial 2-qubit state becomes a Bell state. This behavior demonstrates that even the presence of correlations in the initial state of the ensemble can serve as a resource for enhancing the precision of quantum thermometry, in a similar fashion as to other resources such as local quantum coherence or population unbalance, but with different magnitude as detailed below.

To evaluate the relative enhancement on the maximum QFI due to the value of η , we use again the quantifier (40) with respect to η considering the $\hat{\rho}_{t-m}$ state (22) of 2

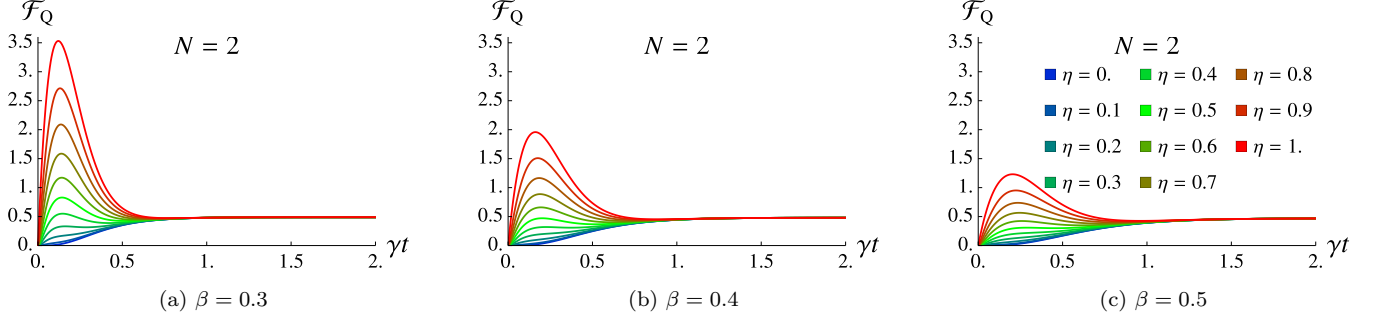


FIG. 7: QFI of the evolved state of a 2-qubit thermometer initialized in the identity-mixed GHZ state $\hat{\rho}_{1-m}$ (19) as a function of time. Different colors correspond to different values of the correlation parameter $\eta \in [0, 1]$.

qubits as the initial state. The quantity $v_\eta(\Phi_\beta^{\otimes 2}, \hat{\rho}_{t-m})$ is plotted as a function of β in Fig. 8, for different values of the local inverse temperature μ of the single-qubit thermometer. We remind that the $\hat{\rho}_{1-m}$ state is recovered when $\mu = 0$. For all the considered values of μ , the quantifier decreases monotonically with increasing β , indicating a reduced influence of correlations on the maximum value of QFI. Thus, at higher bath temperatures (small β) the correlations affect more significantly the value of the QFI's peak; at lower temperatures of the bath, instead, the behavior of the QFI is the opposite. Consistently, the enhancement provided by quantum correlations vanishes for those values of β such that the QFI does not exhibit a maximum in the transient regime, meaning that the largest value of the QFI is reached only asymptotically. The trend of v_η , which quantifies how much correlations are relevant in enhancing the QFI, changes depending on the interplay between the local inverse temperature μ of the thermometers and the inverse temperature β of the bath. The influence of correlations is stronger for small values of μ , although it occurs over a narrower range of β values. Conversely, as μ increases, this effect becomes less pronounced but extends over a broader range: v_η goes through a reduction exceeding 50% in its maximum value for $\mu = 2.5$. Moreover, the value of β at which the gain due to correlations vanishes increases with μ .

Furthermore, we analyze the QFI of two thermometers initialized in the squeezed state defined in Eq. (26). We remind that this state is pure for all values of the squeezing parameter χ , which does not even affect the local populations of the qubits. The QFI of the time-evolved state is shown in Figs. 9a and 9b, as a function of time and of χ for a fixed temperature of the bath. In the plot we consider $\chi \in [0, \pi]$, since the QFI exhibits periodic behavior in the squeezing parameter, with period π . As a side note, we observe that the QFI exhibits a symmetry in the squeezing parameter such that $\mathcal{F}_Q(\hat{\rho}_{sq}(\chi)) = \mathcal{F}_Q(\hat{\rho}_{sq}(\pi - \chi))$. Moreover, the QFI reaches its maximum during the transient for $\chi = n\pi$ with n being an integer number. The value $\chi = n\pi$ implies initializing the two thermometers under scrutiny in either

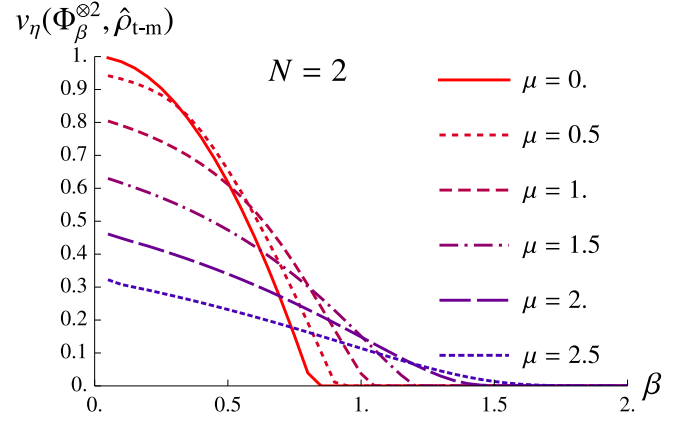


FIG. 8: Relative enhancement $v_\eta(\Phi_\beta^{\otimes 2}, \hat{\rho}_{t-m})$ (40) of QFI w.r.t. the correlation parameter η , as a function of the bath inverse temperature β . Initial state: thermal-mixed GHZ state modified by thermal weights $\hat{\rho}_{t-m}$ (22). Different colors correspond to different values of the thermometers' inverse temperature μ . For $\mu = 0$, the initial state of the ensemble reduces to the identity-mixed GHZ state $\hat{\rho}_{1-m}$ (19), meaning that the curve for $\mu = 0$ represents the quantity $v_\eta(\Phi_\beta^{\otimes 2}, \hat{\rho}_{1-m})$.

of the pure states $|+\rangle^{\otimes 2}$ or $|-\rangle^{\otimes 2}$, whereby the enhancement in the estimation precision is due to the presence of quantum coherence in the initial state (see Sec. VB).

An additional increase in the height of the transient peak in the QFI is observed for $\chi = \pi/2$, which corresponds of preparing the thermometers in a rotated $|\text{GHZ}_2\rangle$ state at the beginning of the thermometry protocol. In such case, the presence of quantum correlations in the early stages of the thermalization dynamics is responsible for the peak in the QFI. Therefore, the interplay between quantum coherence and correlations can account for the results of the numerical simulations shown in Figs. 9a and 9b. The figures show that when the peak is mainly due to quantum correlations, it emerges earlier in time compared to peaks that mainly depend on quantum coherence. We also carried out a similar analysis for

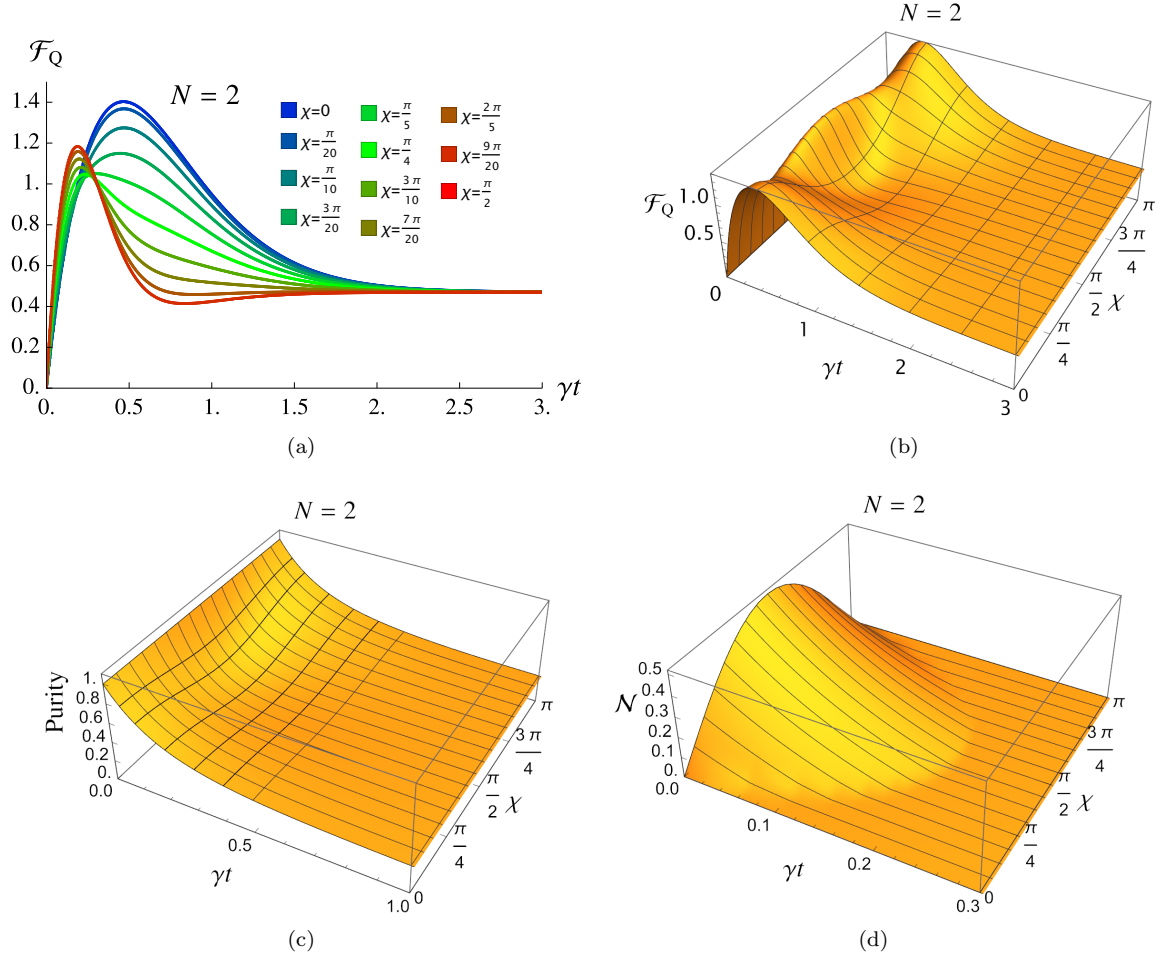


FIG. 9: Panels (a)-(b): QFI associated to two thermometers' state, initialized in the squeezed state of Eq. (26), as a function of the time and the squeezing parameter χ . Panels (c)-(d): Purity and negativity of entanglement (defined in Eq. (37)), respectively, of the two thermometers' state, as a function of time and of the squeezing parameter χ . The inverse temperature of the bath is fixed at $\beta = 0.5$.

the rotated squeezed states with $\theta = \{\pi/4, \pi/2, 3\pi/4\}$, observing distinct behaviors for $\chi \in [0, 2\pi]$, and also initializing the thermometers in the k -GHZ superposition states (24) with $k = \{0, 1, +, -, \ell, r\}$ (refer to III). The interplay between quantum coherence and correlations found in these settings is comparable with the ones reported above.

Finally, in order to isolate the effect of correlations, in Fig. 10 we compare the behavior in time of the QFI of two-qubit thermometers prepared respectively in the squeezed state $\hat{\rho}_{\text{sq}}(\chi)$ and in the initial state given by the tensor product of the reduced states of $\hat{\rho}_{\text{sq}}(\chi)$. Formally, the two initial states we are comparing are $\hat{\rho}_{\text{sq}}(\chi)$ and $\hat{\rho}_{\text{sqp}}(\chi) \equiv \text{Tr}_{S_2}[\hat{\rho}_{\text{sq}}(\chi)] \otimes \text{Tr}_{S_1}[\hat{\rho}_{\text{sq}}(\chi)]$, where S_1 and S_2 stand for the first and second thermometer respectively. In Fig. 10 we plot the difference $\mathcal{F}_Q(\Phi_\beta^{(t)}[\hat{\rho}_{\text{sq}}(\chi)]) - \mathcal{F}_Q(\Phi_\beta^{(t)}[\hat{\rho}_{\text{sqp}}(\chi)])$ as a function of time for different values of the squeezing parameter χ . The plot shows that the difference in the estimation

precision between the two initial states increases (during the transient) as χ approaches $\pi/2$, namely for a larger amount of correlation in the squeezed state. Conversely, when the squeezing parameter deviates from $\pi/2$, the time-behavior of the QFI's curves becomes progressively more similar, eventually coinciding for $\chi = n\pi$ (n integer number) whereby $\hat{\rho}_{\text{sqp}}(\chi)$ corresponds to $\hat{\rho}_{\text{sq}}(\chi)$.

D. Explanation in terms of purity, local temperature and negativity of entanglement

A general qualitative explanation for the behavior of the QFI can be framed also in terms of the purity and quantum correlations present in the initial state of the ensemble of thermometers, and their corresponding behavior during the time evolution under the action of the GAD channel. If the temperature of the bath is high enough to allow the appearance of a QFI peak during the

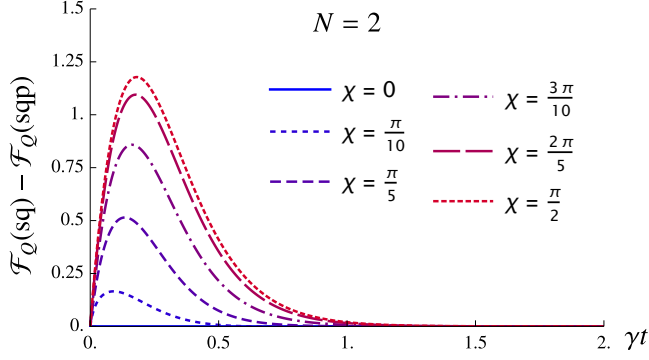


FIG. 10: Enhancement of estimation precision $\mathcal{F}_Q(\Phi_\beta^{(t)}[\hat{\rho}_{\text{sq}}(\chi)]) - \mathcal{F}_Q(\Phi_\beta^{(t)}[\hat{\rho}_{\text{sqp}}(\chi)])$ due to quantum correlations in a squeezed initial state (26), as a function of time, for different values of the squeezing parameter χ ; $\hat{\rho}_{\text{sqp}}(\chi) = \text{Tr}_{S_2}[\hat{\rho}_{\text{sq}}(\chi)] \otimes \text{Tr}_{S_1}[\hat{\rho}_{\text{sq}}(\chi)]$.

transient, this peak can be attributed to either (i) preserved quantum correlations or (ii) a level of state purity that exceeds the asymptotic thermal value associated to the thermometers' state. This phenomenon is illustrated in Figs. 9 and 11, which show the time evolution of the QFI, the purity and the negativity of entanglement [see Eq. (37)] for both the squeezed state (Eq. (26), Fig. 9) and the k-GHZ superposition state $\hat{\rho}_{\text{k-s}}(\alpha, +)$ (Eq. (24), Fig. 11). The curves in the figures are plotted as a function of time and of a tunable parameter (χ and α , respectively) of the initial state. One can observe that a local or global peak in the QFI is due necessarily to the behavior of the negativity of entanglement and the purity of the thermometers' state.

In accordance with this evidence, our analysis shows that initializing the thermometers in the maximally mixed state $\mathbb{1}_{2^N}/2^N$ yields no QFI peak during the transient, as no quantum correlations are present and the purity takes the minimum value. Finally, we observe that the peaks of QFI associated with correlations among the thermometers of the ensemble occur earlier in time than those driven by the purity of their state.

E. Bound and scaling of QFI with N

Using the representation of the GAD quantum channel in Eq. (6), the operator \hat{M}_2 is found to be the 2×2 null matrix (see Appendix C for the calculation). Hence, the bound (35) depends solely on the coefficient $\|\hat{M}_1\|$, minimized over the equivalent Kraus representations of the channel. The fact that $\|\hat{M}_2\| = 0$ is a sufficient condition to prevent a superlinear scaling of the QFI with the number of thermometers N . Therefore, the best possible scaling of the QFI for large N in this scenario is limited to be linear with a specific slope. However, this does not mean necessarily that, for small values of N and specific initial states, the trend of the QFI with N is exactly fit-

ted by the same linear curve, because of finite-size effects that cause small deviations from the value obtained in the large- N limit.

In spite of the scaling constraint for large N , in Fig. 12 we investigate how the enhancement in the QFI (compared to the corresponding value at the thermal state) changes with the number N of thermometers, considering the initial states $\hat{\rho}_{\text{gs}}$, $\hat{\rho}_{\text{t-m}}(\eta = 0.5, \mu = 1)$, $\hat{\rho}_{\text{1-m}}(\eta = 1)$, $\mathbb{1}_{2^N}/2^N$, and setting a fixed temperature of the bath. All the points plotted in the figure are values of the QFI taken at a specific time t^* , which is the time when the evolved state of an ensemble of 6 thermometers achieves the maximum value of the QFI. This choice is based on the analysis of the times at which the QFI reaches a peak. For $N > 4$, indeed, the peak of the QFI occurs approximately at the same time t^* . Therefore, we have selected the time corresponding to the peak of the QFI associated to the largest number of thermometers we considered.

In Fig. 12 we show a linear fit of the QFI values at $t = t^*$ for N thermometers prepared in the different states mentioned above; the numerical values of the slopes and the corresponding standard errors are reported in the caption. Initializing the thermometers' ensemble in the product states $\hat{\rho}_{\text{gs}}$ and $\mathbb{1}_{2^N}/2^N$, the scaling of the QFI with N is strictly linear due to the additivity property of the QFI for separable states. Among all the states we considered, the ground state gives the best performance, yielding the steepest slope of the linear fit. In contrast, the (normalized) identity state gives the worst performance, since the corresponding QFI does not exhibit any peak during the transient of the thermalization dynamics. The optimal strategy in this case is to wait until thermalization is complete, and then perform the thermometry at equilibrium. Thus, the plot corresponding to the initial identity state provides a figure of merit for the precision achievable by means of equilibrium thermometry for the estimation of β . This means that Fig. 12 highlights the advantage of the non-equilibrium approach over equilibrium thermometry in the context of estimating a parameter defining the GAD channel.

A particularly interesting behavior of the QFI is observed for initially correlated states. Although an overall linear scaling of the QFI with the number of thermometers is expected for large N , as constrained by the bound in Eq. (35), for small N we observe a scaling of the QFI that can be considered slightly superlinear. However, as the number of thermometers increases, the QFI already exhibits a linear behavior with N , which is characterized by a specific slope that holds up to the large- N limit.

VI. CONCLUSIONS

In this paper, we have studied the metrological limits for performing thermometry of a macroscopic thermal bath using an ensemble of qubit thermometers whose global state is initially correlated. In our analysis, we have assumed that the thermometers interact weakly

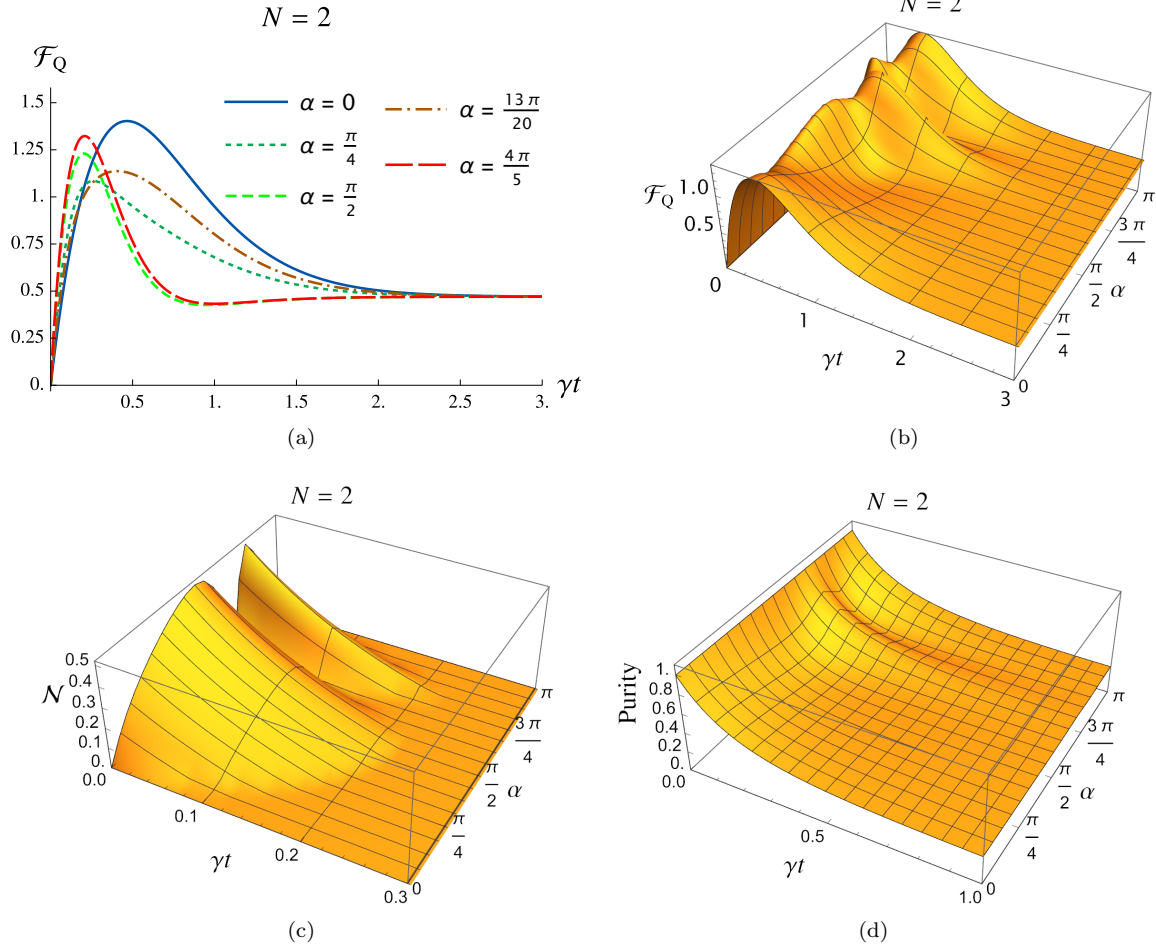


FIG. 11: Panels (a)-(b): QFI associated to two thermometers' state, initialized in the $+$ -GHZ state of Eq. (24) with $|k\rangle = |+\rangle$, as a function of the time and the parameter α . Panels (c)-(d): Purity and negativity of entanglement (defined in Eq. (37)), respectively, of the two thermometers' state, as a function of time and of the parameter α . The inverse temperature of the bath is fixed at $\beta = 0.5$.

with the bath. In doing this, we focused on the time behavior of the QFI associated with the thermometers' state as they thermalize toward the thermal state at the same temperature as the bath.

We determine that performing quantum thermometry during the transient of the thermalization dynamics is highly advantageous compared to carrying it out once the quantum thermometers have reached equilibrium with the thermal bath. This advantage stems from the possibility of exploiting quantum resources such as the quantum correlations among the thermometers, which are assumed to be initially present before their interaction with the bath. We also investigate in detail the effect on the QFI of different bath temperatures, as well as local features of each thermometer's state, such as local coherence and population terms.

Our findings indicate that there exist ranges of values for each of these quantities that can lead to an improvement in estimation precision. In particular, specific com-

binations of bath temperature, local coherence, and inter-thermometer correlations can give rise to a transient peak in the QFI that significantly exceeds its asymptotic value after thermalization, thus enabling more precise temperature estimation, provided the measurement is performed out of equilibrium. It is worth stressing that the precision enhancement in nonequilibrium thermometry can only be achieved within a narrow time window, whose position depends on the initially unknown value of the parameter to be estimated, here the temperature of the bath. While this seems to undermine our non-equilibrium approach to quantum thermometry, a possible solution to this challenge is to introduce an initial step based on equilibrium thermometry, which would serve as prior information and yield a first estimate of the bath temperature. Then, this estimate can be used to approximately identify the time interval where the QFI reaches its peak.

The best performance in enhancing thermometry precision is achieved when initializing the ensemble of ther-

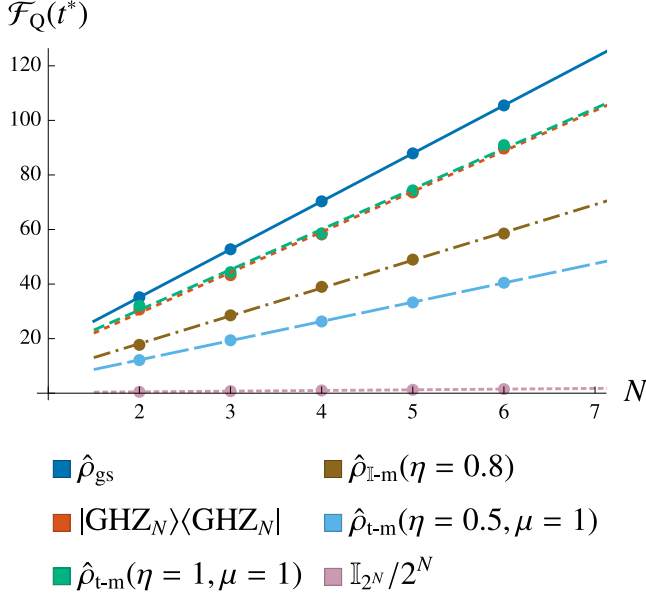


FIG. 12: QFI at time t^* as a function of the number N of thermometers. Different colors and line styles correspond to the initial states of the thermometers shown in the legend. The slopes of the linear fits of the QFI in N for the different initial states are: 17.58 for the $\hat{\rho}_{\text{gs}}$ state, 14.83 ± 0.38 for the $|\text{GHZ}_N\rangle\langle\text{GHZ}_N|$ state, 14.78 ± 0.49 for the $\hat{\rho}_{t-m}(\eta = 1, \mu = 1)$ state, 10.20 ± 0.14 for the $\hat{\rho}_{t-m}(\eta = 0.8)$ state, 7.06 ± 0.04 for the $\hat{\rho}_{t-m}(\eta = 0.5, \mu = 1)$ state, and 0.25 for the $\mathbb{I}_{2^N}/2^N$ state. The errors on the fitted slopes are reported (with two significant digits) only for initially correlated states of the thermometers, since for initially separable states all the values of the QFI are perfectly aligned on a straight curve due to the additivity property of the QFI.

monometers in the state $\hat{\rho}_{\text{in}} = |0\rangle\langle 0|^{\otimes N}$. The downside of this state is that it is thermodynamically challenging to prepare, according to the third law of thermodynamics [46], as it corresponds to a zero-temperature pure state. In spite of this, high-fidelity preparation of low-temperature states has been achieved in specific, well-controlled laboratory settings [47, 48], and the problem is of obvious relevance for quantum computing [49]. Still, initializing the ensemble of thermometers in a quantum-correlated state with a local temperature significantly greater than zero appears quite more feasible.

The main outlook of this work is to design a quantum channel for performing nonequilibrium thermometry such that $\|\hat{M}_2\| \neq 0$ in the bound of Eq. 35. It would be already quite interesting to identify a channel with these characteristics even within a short time window, as it could enable superlinear (i.e., superextensive) scaling of the QFI with the number of thermometers. In this regard, a promising direction would be to consider nonlocal maps, which over time introduce quantum correlations among the thermometers while they undergo

thermalization.

ACKNOWLEDGMENTS

The authors acknowledge very useful discussions with Lorenzo Buffoni, Angelo Carollo, Gonalo Frazao, Seth Lloyd, and Andrea Smirne. We also thank for financial support from the PNRR MUR project PE0000023 NQSTI funded by the European Union—Next Generation EU, the PRIN project 2022FEXLYB “Quantum Reservoir Computing (QuReCo)”, and the European project “High Performance Computer and Quantum Simulator hybrid (HPCQS)” with grant agreement No. 101018180 funded by the European Union’s Horizon 2020 research and innovation programme.

Appendix A: Proof of Eq. (28)

In order to derive the expression of the partial trace given in Eq. (28), let us first focus on the non-rotated squeezed state of Eq. (26). Recall that this state belongs to the bosonic subspace of the N -qubit Hilbert space, and can therefore be expressed as a combination of $N + 1$ orthogonal Fock states:

$$|\psi_{\text{sq}}(\chi)\rangle = \frac{1}{2^{N/2}} \sum_{k=0}^N \sqrt{\binom{N}{k}} e^{-i\chi(\frac{N}{2}-k)^2} |N-k, k\rangle. \quad (\text{A1})$$

Here, the notation $|N-k, k\rangle$ refers to a bosonic Fock state with $N-k$ particles in the qubit state $|0\rangle$ and k particles in the qubit state $|1\rangle$ and $\binom{N}{k}$ denotes the binomial coefficient $N!/[(N-k)!k!]$.

The density operator associated with the squeezed state can thus be expressed as

$$\hat{\rho}_{\text{sq}}(\chi) = \frac{1}{2^N} \sum_{k,k'=0}^N \sqrt{\binom{N}{k}\binom{N}{k'}} e^{i\chi(N-k-k')(k-k')} \times |N-k, k\rangle\langle N-k', k'|. \quad (\text{A2})$$

The partial trace $\hat{\rho}_{\text{sq}}^{(1)}(\chi) = \text{Tr}_{S_{N-1}}[\hat{\rho}_{\text{sq}}(\chi)]$ can now be evaluated by tracing over any subset of $N-1$ qubits, since the state is invariant under particle exchange. To show how this calculation is carried out, we rewrite the Fock state $|N-k, k\rangle$ in a more explicit form:

$$|N-k, k\rangle = \frac{1}{\sqrt{M_{N,k}}} \sum_{P \in S_N} |\psi_{P_1}\rangle \otimes \cdots \otimes |\psi_{P_N}\rangle. \quad (\text{A3})$$

In this equation, P is a permutation in S_N , the symmetric group of order N , $M_{N,k} = N!(N-k)!k!$ is a normalization constant and $|\psi_{P_j}\rangle \in \{|0\rangle, |1\rangle\}$ so that $|0\rangle$ and $|1\rangle$ appear $N-k$ and k times, respectively, in the tensor product.

Using the above equation, we obtain

$$\begin{aligned} \text{Tr}_{S_{\setminus i}}[|N-k, k\rangle\langle N-k', k'|] &= \frac{1}{\sqrt{M_{N,k} M_{N,k'}}} \times \\ &\times \sum_{P, P' \in S_N} |\psi_{P_1}\rangle\langle\psi_{P'_1}| \prod_{j=2}^N \langle\psi_{P_j}|\psi_{P'_j}\rangle, \end{aligned} \quad (\text{A4})$$

where, without loss of generality, we chose to trace over the last $N-1$ qubits. Due to the $N-1$ scalar products that appear in this formula, the partial trace will vanish for all pairs k, k' that do not fulfill the condition $k-k' = 0, \pm 1$. The combination $k-k' = 0$ will provide terms proportional to $|0\rangle\langle 0|$ and $|1\rangle\langle 1|$, while $k-k' = -1$ and $k-k' = 1$ terms proportional to $|0\rangle\langle 1|$ and $|1\rangle\langle 0|$, respectively. Through simple combinatorics, it is possible to derive explicit expressions for all the relevant partial traces in Eq. (A4). By combining these with Eq. A2, we then find

$$\langle 0|\hat{\rho}_{\text{sq}}^{(1)}(\chi)|0\rangle = \frac{1}{2^N} \sum_{k=0}^{N-1} \binom{N-1}{k} = \frac{1}{2}, \quad (\text{A5})$$

$$\langle 1|\hat{\rho}_{\text{sq}}^{(1)}(\chi)|1\rangle = \frac{1}{2^N} \sum_{k=1}^N \binom{N-1}{k-1} = \frac{1}{2}, \quad (\text{A6})$$

$$\begin{aligned} \langle 0|\hat{\rho}_{\text{sq}}^{(1)}(\chi)|1\rangle &= \frac{1}{2^N} \sum_{k=0}^{N-1} \binom{N-1}{k} e^{-i\chi(N-2k-1)} = \\ &= \frac{\cos^{N-1}(\chi)}{2}, \end{aligned} \quad (\text{A7})$$

$$\begin{aligned} \langle 1|\hat{\rho}_{\text{sq}}^{(1)}(\chi)|0\rangle &= \frac{1}{2^N} \sum_{k=1}^N \binom{N-1}{k-1} e^{i\chi(N-2k+1)} = \\ &= \frac{\cos^{N-1}(\chi)}{2}. \end{aligned} \quad (\text{A8})$$

We have thus proved that

$$\rho_{\text{sq}}^{(1)}(\chi) = \frac{1}{2} \begin{pmatrix} 1 & \cos^{N-1}(\chi) \\ \cos^{N-1}(\chi) & 1 \end{pmatrix}, \quad (\text{A9})$$

where $\rho_{\text{sq}}^{(1)}(\chi)$ denotes the matrix representation of the density operator $\hat{\rho}_{\text{sq}}^{(1)}(\chi)$. We now consider the partial trace of the rotated squeezed state, i.e. $\hat{\rho}_{\text{sq}}^{(1)}(\chi, \theta) = \text{Tr}_{S_{\setminus i}}[\hat{\rho}_{\text{sq}}(\chi, \theta)]$. As the rotated state is obtained by applying the local operator $e^{-i\theta\hat{J}_y} = \otimes_{j=1}^N e^{-i\theta(\hat{\sigma}_y^{(j)}/2)}$ to $|\psi_{\text{sq}}(\chi)\rangle$, the partial trace simply transforms as

$$\rho_{\text{sq}}^{(1)}(\chi, \theta) = e^{-i\theta(\sigma_y^{(1)}/2)} \rho_{\text{sq}}^{(1)}(\chi) e^{i\theta(\sigma_y^{(1)}/2)}, \quad (\text{A10})$$

where all operators are in their matrix representation. By making use of our previous result Eq. (A9) and the matrix representation

$$e^{-i\theta(\sigma_y^{(1)}/2)} = \begin{pmatrix} \cos\left(\frac{\theta}{2}\right) & -\sin\left(\frac{\theta}{2}\right) \\ \sin\left(\frac{\theta}{2}\right) & \cos\left(\frac{\theta}{2}\right) \end{pmatrix} \quad (\text{A11})$$

for the rotation of the single-qubit state, we eventually get Eq. (28).

Appendix B: Details on the QFI at thermal equilibrium

It is known [23] that for diagonal states—and thus, in particular, for asymptotic thermal states—the relation (32) holds. We can therefore evaluate the asymptotic value of the QFI from the variance of the thermometer Hamiltonian with respect to the thermal state at the temperature T (inverse temperature $\beta = 1/T$) under consideration. Following Ref. [24], we have

$$\langle \hat{H} \rangle = \varepsilon_0 \pi_0(\beta) + \varepsilon_1 \pi_1(\beta) = \varepsilon_1 - [\varepsilon_1 - \varepsilon_0] \pi_0(\beta) \quad (\text{B1})$$

and therefore

$$\begin{aligned} \Delta^2 \hat{H} &= \left(\langle \hat{H} \rangle - \varepsilon_0 \right)^2 \pi_0(\beta) + \left(\langle \hat{H} \rangle - \varepsilon_1 \right)^2 \pi_1(\beta) = \\ &= \left[(\varepsilon_1 - \varepsilon_0)[1 - \pi_0(\beta)] \right]^2 \pi_0(\beta) \\ &\quad + \left[(\varepsilon_1 - \varepsilon_0)\pi_0(\beta) \right]^2 [1 - \pi_0(\beta)] = \\ &= (\varepsilon_1 - \varepsilon_0)^2 \pi_0(\beta)[1 - \pi_0(\beta)]. \end{aligned} \quad (\text{B2})$$

One can see that the maximum value of the equilibrium QFI is attained for $\pi_0 = \pi_1 = 1/2$, corresponding to the limit of infinite bath temperature, $T \rightarrow +\infty$. In contrast, the QFI vanishes in the zero-temperature limit, $T \rightarrow 0$. This behavior is consistent with that of the non-equilibrium QFI as a function of the bath temperature, as discussed in Sec. V A. Therefore, the limit on the estimation precision for ν repetition of the experiment given by the quantum Cramér-Rao bound becomes

$$\Delta \tilde{\beta} \geq \frac{1}{\hbar \omega \sqrt{\nu \pi_0(\beta)[1 - \pi_0(\beta)]}}, \quad (\text{B3})$$

where we substituted the values for the energy eigenvalues $\varepsilon_{0(1)} = -(+)\hbar\omega/2$.

Appendix C: Proof that \hat{M}_2 is the null matrix

In this section, we show that the QFI of the thermometer ensemble with respect to the bath temperature cannot scale faster than linearly with the number N of thermometers. This result holds for any functional form of the coefficients p and q defining the channel, as the derivation assumes them to be generic functions of the inverse temperature β of the bath $p, q = p(\beta), q(\beta)$.

Using the definition in Eq. (36), we compute the matrix \hat{M}_2 , whose operator norm determines the coefficient of the quadratic term in the QFI upper bound given in Eq. (35).

The derivatives of the adjoint Kraus operators turn out

to be

$$\begin{aligned}
\partial_\beta \hat{K}_1^\dagger &= \begin{pmatrix} \frac{\partial_\beta q}{2\sqrt{q}} & 0 \\ 0 & -\frac{\partial_\beta p}{2\sqrt{1-p}}\sqrt{q} + \frac{\partial_\beta q}{2\sqrt{q}}\sqrt{1-p} \end{pmatrix}, \\
\partial_\beta \hat{K}_2^\dagger &= \begin{pmatrix} 0 & 0 \\ \frac{\partial_\beta p}{2\sqrt{p}}\sqrt{q} + \frac{\partial_\beta q}{2\sqrt{q}}\sqrt{p} & 0 \end{pmatrix}, \\
\partial_\beta \hat{K}_3^\dagger &= \begin{pmatrix} -\frac{\partial_\beta p}{2\sqrt{1-p}}\sqrt{1-q} - \frac{\partial_\beta q}{2\sqrt{1-q}}\sqrt{1-p} & 0 \\ 0 & -\frac{\partial_\beta q}{2\sqrt{1-q}} \end{pmatrix}, \\
\partial_\beta \hat{K}_4^\dagger &= \begin{pmatrix} 0 & \frac{\partial_\beta p}{2\sqrt{p}}\sqrt{1-q} - \frac{\partial_\beta q}{2\sqrt{1-q}}\sqrt{p} \\ 0 & 0 \end{pmatrix}. \quad (C1)
\end{aligned}$$

Therefore, one can evaluate the contribution to \hat{M}_2 of each Kraus operator:

$$\begin{aligned}
\partial_\beta(\hat{K}_1^\dagger)\hat{K}_1 &= \frac{1}{2}\partial_\beta \begin{pmatrix} q & 0 \\ 0 & q(1-p) \end{pmatrix}, \\
\partial_\beta(\hat{K}_2^\dagger)\hat{K}_2 &= \frac{1}{2}\partial_\beta \begin{pmatrix} 0 & 0 \\ 0 & pq \end{pmatrix}, \\
\partial_\beta(\hat{K}_3^\dagger)\hat{K}_3 &= \frac{1}{2}\partial_\beta \begin{pmatrix} (1-p)(1-q) & 0 \\ 0 & -q \end{pmatrix}, \\
\partial_\beta(\hat{K}_4^\dagger)\hat{K}_4 &= \frac{1}{2}\partial_\beta \begin{pmatrix} p(1-q) & 0 \\ 0 & 0 \end{pmatrix}. \quad (C2)
\end{aligned}$$

Finally, we obtain

$$\hat{M}_2 = i \sum_a \partial_\beta(\hat{K}_a^\dagger)\hat{K}_a = \frac{i}{2}\partial_\beta \begin{pmatrix} 1 & 0 \\ 0 & 0 \end{pmatrix} = \begin{pmatrix} 0 & 0 \\ 0 & 0 \end{pmatrix}. \quad (C3)$$

While this result does not exclude the possibility of equivalent Kraus representations for which the operator norm of \hat{M}_2 is nonzero, the minimization over all representations in the bound (35) ensures that our result still provides a sufficient condition to limit the scaling with N to being linear.

-
- [1] V. Giovannetti, S. Lloyd, and L. Maccone, Quantum metrology, *Phys. Rev. Lett.* **96**, 010401 (2006).
- [2] V. Giovannetti, S. Lloyd, and L. Maccone, Advances in quantum metrology, *Nat. Photonics* **5**, 222 (2011).
- [3] C. L. Degen, F. Reinhard, and P. Cappellaro, Quantum sensing, *Rev. Mod. Phys.* **89**, 035002 (2017).
- [4] J. Aasi and al., Enhanced sensitivity of the LIGO gravitational wave detector by using squeezed states of light, *Nat. Photonics* **7**, 613 (2013).
- [5] V. Montenegro, C. Mukhopadhyay, R. Yousefjani, S. Sarkar, U. Mishra, M. G. Paris, and A. Bayat, Review: Quantum metrology and sensing with many-body systems, *Phys. Rep.* **1134**, 1 (2025).
- [6] M. Mehboudi, A. Sanpera, and L. A. Correa, Thermometry in the quantum regime: Recent theoretical progress, *J. Phys. A: Math. Theor.* **52**, 303001 (2010).
- [7] P. Abiuso, P. Andrea Erdman, M. Ronen, F. Noé, G. Haack, and M. Perarnau-Llobet, Optimal thermometers with spin networks, *Quantum Sci. Technol.* **9**, 035008 (2024).
- [8] M. Brunelli, S. Olivares, and M. G. A. Paris, Qubit thermometry for micromechanical resonators, *Phys. Rev. A* **84**, 032105 (2011).
- [9] M. Brunelli, S. Olivares, M. Paternostro, and M. G. A. Paris, Qubit-assisted thermometry of a quantum harmonic oscillator, *Phys. Rev. A* **86**, 012125 (2012).
- [10] V. Montenegro, M. G. Genoni, A. Bayat, and M. G. A. Paris, Mechanical oscillator thermometry in the nonlinear optomechanical regime, *Phys. Rev. Res.* **2**, 043338 (2020).
- [11] S. Jevtic, D. Newman, T. Rudolph, and T. M. Stace, Single-qubit thermometry, *Phys. Rev. A* **91**, 012331 (2015).
- [12] S. Razavian, C. Benedetti, M. Bina, A.-K. Y., and M. G. A. Paris, Quantum thermometry by single-qubit dephasing, *Eur. Phys. J. Plus* **134**, 284 (2019).
- [13] W. K. Tham, H. Ferretti, A. V. Sadashivan, and A. M. Steinberg, Simulating and Optimising Quantum Thermometry Using Single Photons, *Sci. Rep.* **6**, 38822 (2016).
- [14] L. Mancino, M. Sbroscia, I. Gianani, E. Rocca, and M. Barbieri, Quantum Simulation of Single-Qubit Thermometry Using Linear Optics, *Phys. Rev. Lett.* **118**, 130502 (2017).
- [15] C. Sabín, A. White, L. Hackermuller, and I. Fuentes, Impurities as a quantum thermometer for a Bose-Einstein condensate, *Sci. Rep.* **4**, 1 (2014).
- [16] T. H. Johnson, F. Cosco, M. T. Mitchison, D. Jaksch, and S. R. Clark, Thermometry of ultracold atoms via nonequilibrium work distributions, *Phys. Rev. A* **93**, 053619 (2016).
- [17] M. T. Mitchison, T. Fogarty, G. Guarnieri, S. Campbell, T. Busch, and J. Goold, In Situ Thermometry of a Cold Fermi Gas via Dephasing Impurities, *Phys. Rev. Lett.* **125**, 080402 (2020).
- [18] A. Sultanov, M. Kuzmanović, A. V. Lebedev, and G. S. Paraoanu, Protocol for temperature sensing using a three-level transmon circuit, *Appl. Phys. Lett.* **119**, 14 (2021).
- [19] O. P. de Sá Neto, H. A. S. Costa, G. A. Pratavia, and

- M. C. de Oliveira, Temperature estimation of a pair of trapped ions, *Sci. Rep.* **12**, 1 (2022).
- [20] J.-M. Yang, H. Yang, and L. Lin, Quantum Dot Nano Thermometers Reveal Heterogeneous Local Thermogenesis in Living Cells, *ACS Nano* **5**, 5067 (2011).
- [21] Y. Wu and T. Weil, Recent Developments of Nanodiamond Quantum Sensors for Biological Applications, *Adv. Sci.* **9**, 2200059 (2022).
- [22] Y. Aiache, C. Seida, K. El Anouz, and A. El Allati, Non-markovian enhancement of nonequilibrium quantum thermometry, *Phys. Rev. E* **110**, 024132 (2024).
- [23] V. Cavina, L. Mancino, A. De Pasquale, I. Gianani, M. Sbroscia, R. I. Booth, E. Roccia, R. Raimondi, V. Giovannetti, and M. Barbieri, Bridging thermodynamics and metrology in nonequilibrium quantum thermometry, *Phys. Rev. A* **98**, 050101 (2018).
- [24] G. Frazão, M. Pezzutto, Y. Omar, E. Zambrini Cruzeiro, and S. Gherardini, Coherence-enhanced single-qubit thermometry out of equilibrium, *Entropy* **26**, 568 (2024).
- [25] S. Seah, S. Nimmrichter, D. Grimmer, J. P. Santos, V. Scarani, and G. T. Landi, Collisional Quantum Thermometry, *Phys. Rev. Lett.* **123**, 180602 (2019).
- [26] R. Ravell Rodríguez, M. Mehboudi, M. Horodecki, and M. Perarnau-Llobet, Strongly coupled fermionic probe for nonequilibrium thermometry, *New J. Phys.* **26**, 013046 (2024).
- [27] G. Salvatori, A. Mandarino, and M. G. A. Paris, Quantum metrology in Lipkin-Meshkov-Glick critical systems, *Phys. Rev. A* **90**, 022111 (2014).
- [28] D. M. Greenberger, M. A. Horne, and A. Zeilinger, Going beyond bell's theorem, in *Bell's theorem, quantum theory and conceptions of the universe* (Springer, 1989) pp. 69–72.
- [29] D. M. Greenberger, M. A. Horne, A. Shimony, and A. Zeilinger, Bell's theorem without inequalities, *Am. J. Phys.* **58**, 1131 (1990).
- [30] M. Horodecki and P. Horodecki, Reduction criterion of separability and limits for a class of distillation protocols, *Phys. Rev. A* **59**, 4206 (1999).
- [31] R. F. Werner, Quantum states with Einstein-Podolsky-Rosen correlations admitting a hidden-variable model, *Phys. Rev. A* **40**, 4277 (1989).
- [32] N. Li, S. Luo, and Y. Sun, Information-theoretic aspects of Werner states, *Ann. Phys.* **424**, 168371 (2021).
- [33] L. Pezzé, A. Smerzi, M. K. Oberthaler, R. Schmied, and P. Treutlein, Quantum metrology with nonclassical states of atomic ensembles, *Rev. Mod. Phys.* **90**, 035005 (2018).
- [34] J. Ma, X. Wang, C. Sun, and F. Nori, Quantum spin squeezing, *Phys. Rep.* **4509**, 89 (2011).
- [35] W. J. Eckner, N. Darkwah Oppong, A. Cao, A. W. Young, W. R. Milner, J. M. Robinson, J. Ye, and A. M. Kaufman, Realizing spin squeezing with Rydberg interactions in an optical clock, *Nature* **621**, 734 (2023).
- [36] M. Kitagawa and M. Ueda, Squeezed spin states, *Phys. Rev. A* **47**, 5138 (1993).
- [37] L. Pezzé and A. Smerzi, Entanglement, nonlinear dynamics, and the Heisenberg limit, *Phys. Rev. Lett.* **102**, 100401 (2009).
- [38] C. Helstrom, Minimum mean-squared error of estimates in quantum statistics, *Phys. Lett. A* **25**, 101 (1967).
- [39] J. Liu, H. Yuan, X.-M. Lu, and X. Wang, Quantum fisher information matrix and multiparameter estimation, *J. Phys. A: Math. Theor.* **53**, 023001 (2019).
- [40] Interestingly, the standard thermometry scheme that involves measurements of the mean energy and error propagation is sufficient to saturate the lower bound in Eq. (29) when applied to thermal states (and to any state diagonal in the Hamiltonian eigenbasis) [23].
- [41] J. Kołodyński and R. Demkowicz-Dobrzański, Efficient tools for quantum metrology with uncorrelated noise, *New J. Phys.* **15**, 073043 (2013).
- [42] R. Demkowicz-Dobrzański, J. Kołodyński, and M. Guţă, The elusive Heisenberg limit in quantum-enhanced metrology, *Nat. Commun.* **3**, 1063 (2012).
- [43] A. Fujiwara and H. Imai, A fibre bundle over manifolds of quantum channels and its application to quantum statistics, *J. Phys. A: Math. Theor.* **41**, 255304 (2008).
- [44] R. Horodecki, P. Horodecki, M. Horodecki, and K. Horodecki, Quantum entanglement, *Rev. Mod. Phys.* **81**, 865 (2009).
- [45] W. R. Inc., Mathematica, Version 14.2, champaign, IL, 2024.
- [46] L. Buffoni, S. Gherardini, E. Zambrini Cruzeiro, and Y. Omar, Third Law of Thermodynamics and the Scaling of Quantum Computers, *Phys. Rev. Lett.* **129**, 150602 (2022).
- [47] L. Buffoni and M. Campisi, Cooperative quantum information erasure, *Quantum* **7**, 961 (2023).
- [48] L. Buffoni and M. Campisi, Collective preparation of large quantum registers with high fidelity, *Quantum Sci. Technol.* **10**, 025053 (2025).
- [49] T. P. Harty, D. T. C. Allcock, C. J. Ballance, L. Guidoni, H. A. Janacek, N. M. Linke, D. N. Stacey, and D. M. Lucas, High-fidelity preparation, gates, memory, and read-out of a trapped-ion quantum bit, *Phys. Rev. Lett.* **113**, 220501 (2014).